SLAC – PUB – 3704
June 1985
(T/E)

HADRONIC DECAYS OF THE $\eta_c(2980)$*

The MARK III Collaboration

R.M. Baltrusaitis,[a] D. Coffman, J. Hauser, D.G. Hitlin,
J.D. Richman,[b] J.J. Russell[c] and R.H. Schindler
California Institute of Technology, Pasadena, CA 91125

D.E. Dorfan, R. Fabrizio,[d] F. Grancagnolo,[b] R.P. Hamilton,[e]
C.A. Heusch, L. Köpke, R. Partridge, J. Perrier, H.F.W. Sadrozinski,
M. Scarlatella, T.L. Schalk, A. Seiden and A.J. Weinstein
University of California at Santa Cruz, Santa Cruz, CA 95064

J.J. Becker,[f] G.T. Blaylock, J.S. Brown, H. Cui,[g]
B.I. Eisenstein, G. Gladding, S.A. Plaetzer, A.L. Spadafora,[h]
J.J. Thaler, A. Wattenberg and W.J. Wisniewski
University of Illinois at Urbana-Champaign, Urbana, IL 61801

K.O. Bunnell, R.E. Cassell, D.H. Coward, K.F. Einsweiler,[b]
L. Moss, R.F. Mozley, A. Odian, J.R. Roehrig,[i] W. Toki,
Y. Unno,[j] F. Villa, N. Wermes and D. Wisinski
Stanford Linear Accelerator Center, Stanford, CA 94305

T.H. Burnett, V. Cook, C. Del Papa,[b] A.L. Duncan,
P.M. Mockett, A. Nappi,[k] J.C. Sleeman,[l] and H.J. Willutzki
University of Washington, Seattle, WA 98195

Submitted to *Physical Review D*

---

* This work was supported in part by the Department of Energy, under contracts DE – AC03-76SF00515, DE – AC02-76ER01195, DE – AC03-81ER40050, DE – AM03-76SF00034, and by the National Science Foundation.

Abstract

From a study of 2.7 million J/ψ decays with the MARK III detector at SPEAR, we determine branching ratios for decays of the η_c to $\eta\pi^+\pi^-$, $\pi^\pm K^\mp K_S$, $\pi^+\pi^-\pi^+\pi^-$, $\pi^+\pi^- K^+K^-$, $p\bar{p}$, the previously unobserved modes $\eta'\pi^+\pi^-$, $\pi^0 K^+K^-$, $\bar{K}^{*0}K^\pm\pi^\mp$, $K^{*0}\bar{K}^{*0}$, and new upper limits on $\rho\rho$, $\omega\omega$, $\delta\pi$, $A_2\,\pi$, $f\eta$ and ηKK. When combined, the different measurements of the η_c mass yield (2980.2 ± 1.6) MeV/c^2. In the decays $\eta_c \rightarrow$ *vector vector*, a strong increase of the decay rate with the number of strange quarks in the final state is observed.

1. Introduction

The η_c is expected to have numerous decay modes into two- and three-hadron final states.[1] To lowest order in perturbation theory, the η_c decays through annihilation into two gluons (the annihilations into one gluon and into one photon are forbidden, respectively, by color-SU(3)- and C-invariance). Much information on gluon dynamics can be obtained by studying the systematics of the η_c mesonic decays. For example, the relative contributions of the three different mechanisms relevant to the decays $\eta_c \to VV$ [2] (Fig. 1) can be determined, once all branching ratios to VV final states are measured. Comparison with J/ψ decays, which occur mostly via annihilation into three gluons or one virtual photon,[3] should be particularly interesting.[4] Thus far only six hadronic decay modes of the η_c had been observed,[5,6,7] with small statistics, and a single measurement of the η_c total hadronic width had been reported.[8]

We present branching ratio measurements for decays of the η_c to $\eta\pi^+\pi^-$, $\pi^\pm K^\mp K_S$, $\pi^+\pi^-\pi^+\pi^-$, $\pi^+\pi^- K^+K^-$, $p\bar{p}$, for the previously unobserved decay modes $\eta'\pi^+\pi^-$, $\pi^0 K^+K^-$, $K^{*0}K^-\pi^+$ (including the conjugate mode $\bar{K}^{*0}K^+\pi^-$), $K^{*0}\bar{K}^{*0}$, and new upper limits for the decays $\rho^0\rho^0$, $\omega\omega$, ηK^+K^-, $A_2^\pm\pi^\mp$, ηf, and $\delta^\pm\pi^\mp$. A new determination of the η_c mass is presented, and limits are set on the η_c total width.

Section II of this paper concerns the experimental details of the analysis and determination of branching ratios. In Section III, we discuss interpretations of the data.

2. Details of the Analysis

The Mark III spectrometer is a general purpose magnetic detector designed for detailed studies of exclusive final states in the SPEAR energy region. The detector is described in detail elsewhere.[9] We limit ourselves here to a brief description of the relevant features. The axial and transverse views of the detector are shown in Fig. 2. A low mass inner drift chamber surrounding the beryllium beam pipe provides tracking and a first level trigger. The main drift chamber system, in a 0.4 T magnetic field, measures the momentum of charged tracks over 84% of the solid angle with a resolution of $\sigma_p/p = 0.015\sqrt{1+p^2}$ (p in GeV/c). Two stereo layers and charge division on four of the axial layers provide a measure of the dip angle. Charged particle identification is obtained with a system of 48 time-of-flight (TOF) counters. These counters, which cover 80% of the solid angle, have a time resolution σ_t of ~190 psec for hadrons. This provides a 3σ π/K separation for momenta up to 800 MeV/c.

Between the TOF counters and the solenoid coil is a highly segmented gas sampling calorimeter consisting of 24 layers of alternating proportional counters and 1/2 radiation length lead sheets. Endcap shower counters of similar design extend the photon detection capability to 94% of the solid angle. The shower counters measure photon angles with a resolution σ_θ of 10 mrad and photon energies with a resolution σ_E/E of $0.17/\sqrt{E}$ (E in GeV). The shower counter is fully efficient for photon energies greater than 100 MeV. This feature is crucial for the reconstruction of $J/\psi \to \gamma\,\eta_c$ decays whose radiative photon has an energy of 114 MeV in the J/ψ rest frame.

We now turn to a discussion of the details of the analysis for each channel. Branching ratios and upper limits obtained from our sample of 2.7 million produced J/ψ's are given in Table 1.

2.1 $\eta_c \to \eta\pi^+\pi^-$

The η is identified by its decay into two photons, and candidate events with the topology $\gamma\gamma\gamma\pi^+\pi^-$ are selected. The identification of photons is difficult because charged particles often interact in the shower counters producing clusters of hits ("split-offs") which can be mistaken for photon signals. The energy distribution of split-offs peaks at zero, and its tail extends up to ~ 600 MeV. To minimize the confusion between real photons and split-offs, only the three highest energy showers are used in the reconstruction, and the energy of each additional photon, if any, is required to be less than 20 MeV. The events are kinematically fitted by imposing energy and momentum constraints (4C-fit). At least one of the three $\gamma\gamma$ effective mass combinations must lie within 30 MeV/c^2 of the η mass. A five constraint (5C) fit to $J/\psi \to \gamma\eta\,\pi^+\pi^-$, $\eta \to \gamma\gamma$ is then applied. The combination with the highest confidence level is retained, and the χ^2-probability is required to be larger than 0.04. The distribution of the cosine of the angle (θ) between the photons and η momentum directions in the η center of mass system is expected to be uniform. Fake η's reconstructed from a low energy split-off and a real photon have values of $|\cos\theta|$ close to one. These background events are removed by the cut $|\cos\theta| < 0.94$. All three $\gamma\gamma$ effective mass combinations must satisfy $|m_{\gamma\gamma} - m_{\pi^0}| > 30$ MeV/c^2.

The $\eta\pi^+\pi^-$ effective mass distribution is shown in Fig. 3. A prominent peak (75 ± 9 events) is observed at the mass of the η_c. Two features, common to most of the channels analyzed, characterize the shape of the background: a peak centered at the mass of the J/ψ and a background which decreases slowly with increasing mass. The J/ψ peak is due to non-radiative J/ψ decays; its tails extend into the η_c mass region. A fit to a Breit-Wigner curve, convoluted with a Gaussian to take into account the mass resolution of 20 MeV/c^2, plus a polynomial for the background[10] yields a mass of (2977 ± 4) MeV/c^2 and a width equal to (11 ± 16) MeV/c^2 for the η_c. Because of the presence of background under the η_c peak, the observation of possible two-body intermediate states is difficult. There is no

evidence for the decays: $\eta_c \to \delta^{\pm}\pi^{\mp}$, $\delta^{\pm} \to \eta\pi^{\pm}$, and $\eta_c \to f\eta$, $f \to \pi^+\pi^-$. Upper limits for these decay modes are given in Table 1.

The reconstruction efficiency is obtained from a detailed Monte Carlo simulation of the detector. The angle (θ) between the e^+ and η_c directions in the laboratory is generated according to a $1 + \cos^2\theta$ distribution, and a uniform phase space distribution is used for the three-body decay $\eta_c \to \eta\pi^+\pi^-$ (the detection efficiency depends only weakly on this assumption. This is true for all three-body decay modes analyzed here.) As the Monte Carlo simulation does not accurately simulate split-offs, the loss associated with the use of the three highest energy showers and the energy cut on all additional photons, $(37 \pm 9)\%$, is determined by measuring the fraction of events with additional photons, and the energy distribution of these photons, in two clean samples of $J/\psi \to \gamma\eta', \eta' \to \eta\,\pi^+\pi^-$ and $J/\psi \to \rho^0\pi^0$ decays. The product of branching rations $B(J/\psi \to \gamma\eta_c) \times B(\eta_c \to \eta\,\pi^+\pi^-)$ is given in Table 1. The systematic error, which has been combined quadratically with the statistical error in Table 1, includes contributions from the Monte Carlo simulation of the detector (10%), the photon selection and the split-off energy cut (10%), the uncertainty in the background subtraction (10%), the total number of produced J/ψ's (5.8%),[11] and the reported uncertainty in the branching ratio $B(\eta \to \gamma\gamma)$, all added in quadrature.

2.2 $\eta_c \to \pi^0K^+K^-$ AND $\eta_c \to \pi^{\pm}K^{\mp}K_S$

The decay $\eta_c \to \pi^0K^+K^-$ is observed in the final state topology $\gamma\gamma\gamma\,K^+K^-$. The selection of photons is identical to that used for the $\eta\pi^+\pi^-$ channel (Section 2.1). The energies of the showers associated with the two charged tracks are required to be less than 1.1 GeV to reject background events produced by Bhabha scatterings. Both kaons are identified by the TOF system ($|\,t_{\rm measured} - t^K_{\rm predicted}\,| \leq 3\sigma$ where σ is the TOF resolution for hadrons). A 4C-fit to $\gamma\gamma\gamma K^+K^-$ is applied, and at least one photon pair is required to have an effective mass equal to that of the π^0 (within 25 MeV/c^2). The photon pair with effective mass

closest to the π^0 mass is used in a 5C-fit to $J/\psi \to \gamma\pi^0 K^+K^-, \pi^0 \to \gamma\gamma$. Events whose χ^2-probability is less than 0.05 are rejected. The direct decay $J/\psi \to K^{*\pm}K^{\mp}, K^{*\pm} \to K^{\pm}\pi^0$ has a large branching ratio[12] and is the main source of background, as low energy split-offs are easily mistaken by the 5C-fit for the radiative photon produced in the decay $J/\psi \to \gamma\eta_c$. To suppress this background, the momentum of each kaon is required to be less than 1.3 GeV/c.

The $K^+K^-\pi^0$ effective mass is presented in Fig. 4. The number of $J/\psi \to \gamma\eta_c$, $\eta_c \to \pi^0 K^+K^-$ events is estimated from a fit to a constant (for the background) plus a Breit-Wigner convoluted with a Gaussian to take into account the mass resolution. The uncertainty in the background shape results in a large systematic error on the number of events, and forbids determination of the η_c width. The amount of background at the η_c mass hinders the observation of the two-body decays $\eta_c \to K^{*\pm}K^{\mp}$. The reconstruction efficiency, $(16 \pm 2)\%$, is obtained from the Monte Carlo simulation; a uniform phase space distribution is assumed for the decay $\eta_c \to \pi^0 K^+K^-$. The loss associated with the photon selection, $(39 \pm 7)\%$, is estimated from the effect of the same selection on the sample of $J/\psi \to K^{*\pm}K^{\pm}$, $K^{*\pm} \to K^{\pm}\pi^0$ events.

We now turn to the analysis of the $\eta_c \to \pi^{\pm}K^{\mp}K_S$ channel. The K_S is identified by its decay to $\pi^+\pi^-$. The first selection requires one to five photon candidates in the shower counters and at least one pair of tracks, assumed to be pions, whose effective mass is consistent with that of the K_S within 50 MeV/c^2. If so, one of the two remaining tracks has to be identified as a kaon by the TOF system. To remove background events from channels containing π^0's or η's, a cut is made on the variable $U = E_{\rm miss} - P_{\rm miss}$ ($E_{\rm miss}$ and $P_{\rm miss}$ are the missing energy and momentum calculated from all the charged tracks[5]), $|U| \leq 0.2$ GeV. The K_S selection proceeds in the following way: pairs of tracks in the K_S mass range are required to have a vertex displaced by more than 1 mm from the interaction point in the plane perpendicular to the beams. The angle between the momentum vector of the two tracks and the vertex displacement vector (with respect to the interaction point) must be smaller than 11°. If more

than one good K_S candidate is found, the one with mass closest to the K_S mass is kept. A 4C-fit to the hypothesis $J/\psi \to \gamma\pi^+\pi^-K^\pm K^\mp$ is applied, and the χ^2-probability is required to be greater than 0.05. The channels $J/\psi \to \pi^+\pi^-K^\pm\pi^\mp$ and $J/\psi \to \gamma\gamma\pi^+\pi^-K^\pm\pi^\mp$ are the major sources of background. Cuts on the χ^2-probability of 4C-fits to $\pi^+\pi^-K^\pm\pi^\mp$ ($prob(\chi^2) \leq 0.001$) and $\gamma\gamma\pi^+\pi^-K^\pm\pi^\mp$ ($prob(\chi^2) \leq 0.02$) remove most of these background events. The $\pi^+\pi^-$ effective mass distribution for the pair of tracks selected as K_S is shown in Fig. 5, and the $\pi^\pm K^\mp K_S$ effective mass distribution is presented in Fig. 6. Note that all background events from $J/\psi \to \pi^\pm K^\mp K_S$ decays have been removed. The mass of the η_c and the number of events (Table 1) are determined as in Section 2.1. The large systematic error reflects the uncertainty in the background shape. The observation of two-body intermediate states, $\eta_c \to K^{**\pm}K^\mp$ or $\eta_c \to K^{**0}K_S$, is hindered by the presence of background events and the small number of $\eta_c \to \pi^\pm K^\mp K_S$ events. The Monte Carlo simulation assumes a phase space distribution for the three-body decay of the η_c. The ratio of branching ratios $B(\eta_c \to \pi^0K^+K^-)/B(\eta_c \to \pi^\pm K^\mp K_S)$ is 0.7 ± 0.3, in agreement with the value 0.5 expected from isospin symmetry.

2.3 $\eta_c \to \eta'\pi^+\pi^-$

In this channel, the η' is identified by its decay $\eta' \to \gamma\rho^0$ where $\rho^0 \to \pi^+\pi^-$. As split-offs are produced close to charged tracks, showers are ignored when their angle to the closest charged track is smaller than 18°. Events with two or three photons are selected from our four-prong sample and fitted to the hypothesis $J/\psi \to \gamma\gamma\pi^+\pi^-\pi^+\pi^-$. The χ^2-probability is required to be larger than 0.02. The background is reduced by two cuts: energies greater than 60 MeV for the two selected photons and smaller than 60 MeV for the additional one, if any. At this stage of the analysis, most of the events in the sample are $J/\psi \to \pi^0\pi^+\pi^-\pi^+\pi^-$ or $J/\psi \to \eta\pi^+\pi^-\pi^+\pi^-$ decays. These are removed by requiring the two-photon effective mass to be different from m_{π^0} and m_η by more than 65 MeV/c^2. The effective mass distribution of the $\gamma\pi^+\pi^-$ triplet whose $\pi^+\pi^-$ effective mass is

the closest to that of the ρ^0 is shown in Fig. 7. The peak at the η' mass corresponds to the decays $J/\psi \to \gamma\eta'\pi^+\pi^-$, $\eta' \to \gamma\rho^0$, $\rho^0 \to \pi^+\pi^-$. However, as most of the events have more than one $\pi^+\pi^-$ pair consistent with a ρ^0 (partly because of the large ρ^0 width), the combination with the smallest distance δ[13] to the $(m_{\rho^0}, m_{\eta'})$ point in the $(m_{\pi^+\pi^-}, m_{\gamma\pi^+\pi^-})$ plane is chosen. In addition, δ is required to be smaller than two to remove background events. Finally, a 5C-fit to $J/\psi \to \gamma\eta'\pi^+\pi^-$, $\eta' \to \gamma\pi^+\pi^-$ is applied, and the χ^2-probability is required to be greater than 0.02. The $\eta'\pi^+\pi^-$ effective mass distribution is presented in Fig. 8. To study the mass distribution of the background, the η' mass is changed by $\pm$ 160 MeV/c^2 in the 5C-fit, and the events are submitted to the same set of cuts. The background shape is smooth, and $\sim$ 1 background event is expected under the η_c peak. The decays $J/\psi \to \rho^0\eta'$ and $J/\psi \to \omega\eta'$ are two potential sources of background. However their branching ratios are small,[12] and their contributions can be neglected. The number of events and the mass of the η_c are given in Table 1. In the calculation of the efficiency, the three-body decay of the η_c is assumed to be uniform in phase space. The loss associated with the cuts on the number of additional photons and their energies, $(7 \pm 6)\%$, is estimated from the effect of the same cuts on our sample of $J/\psi \to \pi^+\pi^-\pi^+\pi^-$ decays.

2.4 $\eta_c \to \pi^+\pi^-\pi^+\pi^-$

The main difficulty in the event selection for this channel is to separate radiative decay $J/\psi \to \gamma\pi^+\pi^-\pi^+\pi^-$ events from $J/\psi \to \pi^0\pi^+\pi^-\pi^+\pi^-$ events in which one of the photons from the π^0 decay is not detected or has a very small energy. Events with four charged tracks and at most two photon showers are selected. Only one of the two photons is allowed to be outside a cone with half-angle 18° around charged tracks and must have a detected energy of at least 10 MeV. A 4C-fit to $\gamma\pi^+\pi^-\pi^+\pi^-$ is applied, and the χ^2-probability is required to be larger than 0.3. Tight cuts on the quantities U and $P_{t_\gamma}^2$ are applied: $|U| \leq 0.03$ GeV and $P_{t_\gamma}^2 \leq 0.0005$ (GeV/c)^2 ($P_{t_\gamma} = 2P_{4\pi}\sin(\chi/2)$ where $P_{4\pi}$ is the magnitude of the four pion momentum vector, and χ is the acollinearity angle between the pho-

ton and the four pion momentum vector.[5]) The U-cut is applied at $\sim 1\sigma$ of the resolution on U. The effect of this cut on the branching ratio is discussed below. According to the Monte Carlo simulation, 74% of $J/\psi \to \gamma\eta_c$, $\eta_c \to \pi^+\pi^-\pi^+\pi^-$ events have a $P^2_{t_\gamma}$ less than 0.0005 GeV/c^2. Finally, all events containing two pairs of tracks whose effective masses are consistent (within 20 MeV/c^2) with the K_S mass are removed. Evidence for the decay $J/\psi \to \gamma\eta_c$, $\eta_c \to \pi^+\pi^-\pi^+\pi^-$ is presented in Fig. 9. The background from the decay process $J/\psi \to \pi^0\pi^+\pi^-\pi^+\pi^-$ can be estimated from the $P^2_{t_\gamma}$ distribution, and has been subtracted.[14] To determine the number of events, the mass distribution is fit using a Gaussian plus a constant background between 2.5 and 3.02 GeV/c^2. The peak at the J/ψ mass, which is produced by $J/\psi \to \pi^+\pi^-\pi^+\pi^-$ decays, has been excluded from the fit. The detection efficiency, $(7.7 \pm 0.8)\%$, is obtained from Monte Carlo simulation assuming a uniform phase space distribution for the decay $\eta_c \to \pi^+\pi^-\pi^+\pi^-$. The loss due to the cuts on the number of photons and on their energies, $(26 \pm 8)\%$, is estimated from a sample of $J/\psi \to \pi^+\pi^-\pi^+\pi^-$ events. The systematic error on the branching ratio takes into account a 20% uncertainty in the number of background events. The branching ratio does not change (within errors) when the U-cut is loosened to $|U| < 0.1$ GeV. A search is made for the two-body decays $\eta_c \to \rho^0\rho^0$, $\rho^0 \to \pi^+\pi^-$ and $\eta_c \to A_2^\pm\pi^\mp$, $A_2^\pm \to \rho^0\pi^\pm$.[14] No signals are observed, and upper limits are given in Table 1.

2.5 $\eta_c \to \pi^+\pi^-K^+K^-$

Four-prong events are required to have at least one track identified as a kaon by the TOF system and one or more photon showers. In this decay mode, the processes $J/\psi \to \pi^+\pi^-K^+K^-$ and $J/\psi \to \pi^0\pi^+\pi^-K^+K^-$ are the main sources of background. A cut is applied on the cosine of the angle (β) between the direction of the photon and the direction of the charged particles total momentum, $\cos\beta \leq -0.8$, to remove background events which contain a π^0. If several photon showers are present, at least one has to satisfy the cut. Note that this cut does not reject $J/\psi \to \pi^+\pi^-K^+K^-$ decays and $J/\psi \to \pi^0\pi^+\pi^-K^+K^-$ events in which

one of the two photons produced in the decay of the π^0 has a very low energy. The particle identification is done in the following way: a 4C-fit to $\gamma\pi^+\pi^-K^+K^-$ is applied (all four possible particle identity assignments are tried), and the sum of chi-squared $\chi^2 = \chi^2_{\text{4C-fit}} + \chi^2_{\text{TOF}}$, where $\chi^2_{\text{TOF}} = \sum_{\substack{\text{charged}\\ \text{tracks}}} \frac{(t_{\text{measured}} - t_{\text{predicted}})^2}{\sigma^2_{TOF}}$, is used to select the best particle identification. A χ^2-probability greater than 0.05 is then required from the 4C-fit to the chosen combination. To remove split-offs, showers are ignored if they lie close to charged tracks (angle to the closest charged track smaller than 11°.) Further background rejection is achieved by two cuts on ratios of χ^2 (the fit hypothesis is given in parentheses):

$$\frac{\chi^2(J/\psi \to \pi^+\pi^-K^+K^-)}{\chi^2(J/\psi \to \gamma\pi^+\pi^-K^+K^-)} \geq 6$$

and

$$\frac{\chi^2(J/\psi \to \pi^0\pi^+\pi^-K^+K^-)}{\chi^2(J/\psi \to \gamma\pi^+\pi^-K^+K^-)} \geq 8 .$$

The $\pi^+\pi^-K^+K^-$ effective mass distribution is shown in Fig. 10a. The η_c can decay via the two- and three-body intermediate states $K^{*0}K^-\pi^+$ (and $\bar{K}^{*0}K^+\pi^-$) and $K^{*0}\bar{K}^{*0}$. The $K^*K\pi$ and $K^{*0}\bar{K}^{*0}$ effective mass distributions are presented in Figs. 10b and 10c; a $K\pi$ pair is considered to be a K^* when $|m_{K\pi} - m_{K^*}| < 80$ MeV/c^2. A peak at the mass of the η_c is evident in all three distributions. A scatterplot of the $K\pi$ effective masses, $m_{K^+\pi^-}$ versus $m_{K^-\pi^+}$, is shown in Fig. 11. Two K^* bands and a cluster of events at their intersection are apparent. The number of nonresonant events ($\pi^+\pi^-K^+K^-$ decays in the $K^*K\pi$ sample of events; $\pi^+\pi^-K^+K^-$ and $K^*K\pi$ decays in the $K^{*0}\bar{K}^{*0}$ sample) is estimated from the total number of events in each of the three peaks and from the effect of the K^*-cut on three samples of $\eta_c \to \pi^+\pi^-K^+K^-$, $\eta_c \to K^*K\pi$ and $\eta_c \to K^{*0}\bar{K}^{*0}$ Monte Carlo generated events. The reconstruction efficiency is estimated separately for the three decay sequences. In the simulation of the decay process $\eta_c \to K^*K\pi$, the $K\pi$ pair is assumed to be in a $J^P = 1^-$ state, with a relative angular momentum $L = 1$ with respect to the K^* (the two-pseudoscalar $K\pi$ system can

be only in a $J^P = 0^+, 1^-, 2^+, 3^-, \ldots$ state. In addition, all $J^P = even^+$ states are forbidden by parity conservation.) The decay $\eta_c \to \pi^+\pi^- K^+K^-$ was generated according to a uniform phase space distribution. The branching ratios are given in Table 1.

2.6 $\eta_c \to \eta K^+K^-$

The analyses of the ηK^+K^- and $\pi^0 K^+K^-$ channels are very similar. The photon selections are identical, and the kaon identifications are slightly different. In the ηK^+K^- channel, one of the two charged tracks has to be identified as kaon ($(|t_{\rm measured} - t^K_{\rm predicted}| \leq 2.4\sigma$, and probability to be a kaon greater than probability to be a pion). One of the three photon pairs must have an effective mass equal to that of the η within 50 MeV/c^2, and, to remove background events from $J/\psi \to \pi^0 K^+K^-$ decays, all three pairs are required to differ by more than 35 MeV/c^2 from the mass of the π^0. No signal is observed at the η_c mass in the ηK^+K^- effective mass distribution, and an upper limit on the branching ratio is given in Table 1. In the calculation of the efficiency, the decay $\eta_c \to \eta K^+K^-$ is assumed to have a uniform phase space distribution, and the samples of $J/\psi \to {\rm K}^{*\pm}{\rm K}^{\mp}, {\rm K}^{*\pm} \to K^\pm\pi^0$ and $J/\psi \to K^{**\pm}{\rm K}^{*\pm}, K^{**\pm} \to K^\pm\pi^0, {\rm K}^{*\pm} \to K^\mp\pi^0$ events are used to estimate the loss associated with the photon selection, $(45 \pm 6)\%$.

2.7 $\eta_c \to \omega\omega$

Events of the type $J/\psi \to \gamma\gamma\gamma\gamma\gamma\pi^+\pi^-\pi^+\pi^-$ are selected by requiring exactly four charged particles and five to seven photon showers, separated from the charged tracks, with energies greater than 10 MeV.[15] A 6C-fit to the hypothesis $J/\psi \to \gamma\pi^0\pi^+\pi^-\pi^0\pi^+\pi^-$, $\pi^0 \to \gamma\gamma$ is applied. All combinations are tried, and the one with the smallest χ^2 is kept. Background events from the process $J/\psi \to \pi^0\pi^0\pi^0\pi^+\pi^-\pi^+\pi^-$ are removed if the χ^2-probability of the fit for this hypothesis is greater than that for $J/\psi \to \gamma 2(\pi^0\pi^+\pi^-)$, or if one of the

additional photons has an energy greater than 80 MeV. Because π^0's are sometimes falsely reconstructed from a high energy photon and a low-energy split-off, events with asymmetric π^0 decays are rejected ($|(E_{\gamma_1} - E_{\gamma_2})/E_{\pi^0}| > 0.9$ for either π^0's). Finally, the χ^2-probability of the 6C-fit is required to be greater than 0.15. Note that the processes $J/\psi \to \omega\omega$ and $J/\psi \to \pi^0\omega\omega$ are forbidden by C-invariance. Thus, the presence of two ω's is direct evidence for the radiative decay $J/\psi \to \gamma\omega\omega$. A $\pi^0\pi^+\pi^-$ triplet is considered to be an ω if its effective mass lies within 30 MeV/c^2 of that of the ω. The $\omega\omega$ effective mass distribution is shown in Fig. 12. The absence of a signal at the η_c mass yields the upper limit given in Table 1.

2.8 $\eta_c \to p\bar{p}$

Events are required to have exactly two charged tracks, at least one identified as a proton ($|t_{\text{measured}} - t^{p}_{\text{predicted}}| < 2.1\sigma$ and $|t_{\text{measured}} - t^{K,\pi}_{\text{predicted}}| > 1.8\sigma$). Background events from the decay process $J/\psi \to \mu^+\mu^-$ are rejected if the total number of hits in the muon system is greater or equal to three. The energies of the showers associated with charged tracks are required to be smaller than 1.1 GeV to remove background events produced by Bhabha scatterings. The direct decay $J/\psi \to p\bar{p}$ is the principal source of background in the mass region of the η_c.[16] To remove these background events, all photon showers are ignored when the angle between the photon direction and the direction of the closest charged track is smaller than 18° for protons, and 26° for antiprotons. Two additional cuts are applied: the χ^2-probability of a 4C-fit to $J/\psi \to p\bar{p}$ has to be smaller than 5×10^{-6}, and the cosine of the angle between the proton and antiproton directions is required to be greater than -0.999. In the mass region of the η_c, the number of background events from the decay $J/\psi \to p\bar{p}\pi^0$ is small since there is little available phase space. The mass of the η_c is greater than the largest $p\bar{p}$ effective mass allowed in the decay $J/\psi \to p\bar{p}\pi^0$. However, mismeasurement of the photon energies can pull the $p\bar{p}$ effective mass higher. For this reason, events containing two photons with effective mass between 0.1 and 0.2 GeV/c^2

are rejected. Finally, a 4C-fit to $J/\psi \to \gamma p\bar{p}$ is applied, and the χ^2-probability is required to be greater than 5×10^{-6}.

The $p\bar{p}$ effective mass distribution is shown in Fig. 13. The number of events in the η_c peak (result of the usual maximum likelihood fit) is 22.9 ± 8.7. The mass resolution was fixed at the value determined by the Monte Carlo simulation, 7 MeV/c^2, and a second order polynomial was used for the background shape. The width Γ_{η_c}, allowed to vary in the fit, is equal to 10.1 MeV/c^2. The likelihood function is integrated over Γ_{η_c} to set 90% confidence level upper and lower limit on the η_c width: $1.9 < \Gamma_{\eta_c} < 43.1$ MeV/c^2. The background shape is a complicated combination of the decreasing mass distribution of nonresonant $J/\psi \to \gamma p\bar{p}$ decays and of the increasing $J/\psi \to p\bar{p}$ mass distribution. To account for these uncertainties, a systematic error seven events is added to the total number of events.

3. Discussion and Summary

Using the branching ratio $B(J/\psi \to \gamma\eta_c) = (1.27 \pm 0.36) \times 10^{-2}$,[6] we obtain the set of η_c branching ratios given in Table 2. Approximately 20% of the η_c decay modes have been observed. For all three-body decay channels, except $K^*K\pi$, the amount of background events and the small statistics forbid the observation of two-body intermediate states. When combined, our different measurements of the η_c mass yield (2980.2 ± 1.6) MeV/c^2.

If flavor-SU(3) symmetry were exact, the reduced branching ratios $\tilde{B}(\eta_c \to \phi\phi)$, $\tilde{B}(\eta_c \to \rho^0\rho^0)$, $\tilde{B}(\eta_c \to \omega\omega)$, and $\frac{1}{2}\tilde{B}(\eta_c \to K^{*0}\bar{K}^{*0})$ would all be equal.[4,17] The results given in Table 1 yield:

$$\frac{\frac{1}{2}\tilde{B}(\eta_c \to K^{*0}\bar{K}^{*0})}{\tilde{B}(\eta_c \to \phi\phi)} = (0.22 \pm 0.13) \tag{3.1}$$

$$\frac{\tilde{B}(\eta_c \to \rho^0\rho^0)}{\tilde{B}(\eta_c \to \phi\phi)} < 0.64 \quad (90\%\ C.L.) \tag{3.2}$$

$$\frac{\tilde{B}(\eta_c \to \omega\omega)}{\tilde{B}(\eta_c \to \phi\phi)} < 0.34 \ \ (90\%\ C.L.). \tag{3.3}$$

The values of these ratios suggest that the $\eta_c \to VV$ reduced decay rate increases with the number of strange quarks in the final state. This SU(3) breaking pattern is very different from the one observed in $J/\psi \to PV$ decays[4,12] whose reduced decay rates decrease with the number of strange quarks in the final state. A detailed understanding of the dynamics of these decays is needed in order to explain these different SU(3) breaking patterns. For example, consider the three different mechanisms relevant to the decay $\eta_c \to VV$ shown in Figure 1. In order to understand Eq.(3.2), it would seem that the graph of Figure 1b must dominate, as it implies:[18]

$$\frac{\tilde{B}(\eta_c \to \rho^0\rho^0)}{\tilde{B}(\eta_c \to \phi\phi)} = \frac{|\psi_\rho(0)|^4}{|\psi_\phi(0)|^4} = \left(\frac{2\ m_\rho^2\ \Gamma(\rho \to e^+e^-)}{9\ m_\phi^2\ \Gamma(\phi \to e^+e^-)}\right)^2 = 0.48 \pm 0.07 \tag{3.4}$$

where $\psi_V(0)$ is the wavefunction at the origin of the vector meson. We have used $\Gamma(V \to e^+e^-) = 16\pi\alpha^2 e_Q^2 |\psi_V(0)|^2/m_V^2$ with $9e_Q^2 = 9,\ 1,\ 2$ for $\rho,\ \omega$ and ϕ, respectively.[19] Similarly,

$$\frac{\tilde{B}(\eta_c \to \omega\omega)}{\tilde{B}(\eta_c \to \phi\phi)} = 0.36 \pm 0.05 \tag{3.5}$$

$$\frac{\tilde{B}(\eta_c \to \omega\phi)}{\tilde{B}(\eta_c \to \phi\phi)} = 0.60 \pm 0.05 \tag{3.6}$$

These results are consistent with the observed dominance of the $\phi\phi$ mode. On the other hand, the fact that $\eta_c \to K^{*0}\bar{K}^{*0}$ is seen at the rate given by Eq.(3.1) implies that the above picture is too simple. It is clear that the diagram of Figure 1b does not contribute to the $K^*\bar{K}^*$ final state, whereas diagrams 1a and 1c can contribute. The three mechanisms can be treated in a purely phenomenological way by noting that while VV final states ($V = \rho,\ \omega,\ \phi$) can arise from all three diagrams, $K^*\bar{K}^*$ can only arise from Figures 1a and 1c, and $\omega\phi$ can arise only from Figure 1b. Eventually, the relative contributions of the three mechanisms could be determined experimentally once all the above modes are measured.

4. Acknowledgements

We would like to thank H.E. Haber and S. Brodsky for helpful discussions. We gratefully acknowledge the dedicated support of SLAC's SPEAR and Linear Accelerator operating staff. We would also like to thank the technical and engineering staffs of group D at SLAC and the collaborating universities. One of us (N.W.) would like to thank the Alexander von Humboldt foundation for support.

References

(a) Present Address: Physics Dept., Univ. of Utah, Salt Lake City, UT 84112, USA

(b) Present Address: CERN, EP, 1211 Geneva 23, Switzerland

(c) Present Address: SLAC, Stanford University, Stanford, CA 94305, USA

(d) Present Address: Applied Technology, Sunnyvale, CA 94086, USA

(e) Present Address: Anadrill/Schlumberger, Sugarland, Texas 77478, USA

(f) Present Address: ESL, Sunnyvale, CA 94088-3510, USA

(g) Present Address: Institute of High Energy Physics, Bejing, China

(h) Present Address: ORSAY, LAL, France

(i) Present Address: Lockheed Research, Palo Alto, CA 94302, USA

(j) Present Address: Phys. Dept., KEK Tsukuba, Ibaraki 305, Japan

(k) On leave of absence from Univ. of Pisa, Pisa, Italy

(l) Present Address: Physics Dept., Northeastern Univ., Boston, MA 02115, USA

1. C. Quigg and J. L. Rosner, Phys. Rev. **D16**, 1497 (1977).

2. We shall denote pseudoscalar and vector mesons by P and V, respectively.

3. E. D. Bloom, Proc. 1981 SLAC Summer Inst. on Part. Phys., SLAC-245 (1982) and references quoted therein.

4. See, for example:
   H.E. Haber and J. Perrier, U.C. Santa Cruz preprint, SCIPP 85/39 (1985), submitted to *Phys. Rev. D.*

5. T.M. Himel *et al.*, *Phys. Rev. Lett.* **45**, 1146 (1980).

6. R. Partridge *et al.*, *Phys. Rev. Lett.* **45**, 1150 (1980).

7. R.M. Baltrusaitis *et al.*, *Phys. Rev. Lett.* **52**, 2126 (1984).

8. F.C. Porter *et al.*, SLAC-PUB-2796 (1981).
   J.E. Gaiser, Ph.D. Thesis, SLAC-255 (1982) (unpublished).

9. D. Bernstein *et al.*, *Nucl. Inst. Meth.* **226**, 301 (1984), and references quoted therein.

10. A detailed discussion of the possible sources of background can be found in J. J. Becker, Ph. D. Thesis, Univ. of Illinois at Urbana-Champaign (1984).

11. R. M. Baltrusaitis *et al.*, *Phys. Rev.* **D32**, 566 (1985).

12. W. Braunschweig *et al.*, *Phys. Lett.* **63B**, 487 (1976).
F. Vannucci *et al.*, *Phys. Rev.* **D15**, 1814 (1977).
M.E.B. Franklin, *Phys. Rev. Lett.* **51**, 963 (1983).
R.M. Baltrusaitis *et al.*, SLAC-PUB-3435, submitted to *Phys. Rev. D.*

13. $\delta = \sqrt{\frac{(m_{\pi^+\pi^-} - m_{\rho^0})^2}{\sigma^2_{\rho^0}} + \frac{(m_{\gamma\pi^+\pi^-} - m_{\eta'})^2}{\sigma^2_{\eta'}}}$ where σ_{ρ^0} and $\sigma_{\eta'}$ are the resolutions on the ρ^0 and η' mass obtained from the Monte Carlo simulation. These resolutions take into account the natural width of the particles and the resolution of the detector.

14. The background subtraction is described in detail in:
R.M. Baltrusaitis *et al.*, SLAC-PUB-3682, submitted to Phys. Rev. D.

15. The details of this analysis can be found in:
R.M. Baltrusaitis *et al.*, SLAC-PUB-3681, submitted to *Phys. Rev. Lett.*

16. A detailed discussion of this analysis can be found in:
J.S. Brown, Ph. D. Thesis, University of Washington (1984) (unpublished).

17. The width $\Gamma(\eta_c \to VV)$ is given by

$$\Gamma(\eta_c \to V\,V) = \frac{1}{32\pi^2\, m_{\eta_c}} \times \left(\frac{P_V}{m_{\eta_c}}\right) \times \sum_{\text{spins}} \int \mid \mathcal{M} \mid^2 d\Omega_V$$

with $\mathcal{M} = g_V\ m_{\eta_c}\ \hat{e}_{V_1} \cdot \hat{e}_{V_2} \times \vec{P}_V$; $\hat{e}_{V_1}$ and $\hat{e}_{V_2}$ are the two vector mesons polarization vectors, and $\vec{P}_V$ is their momentum in the center of mass of the η_c. The quantities g_V and P_V depend on the particular final state. To factor out the P_V dependence, we shall use the reduced branching ratio

$\tilde{B}(\eta_c \to V\,V) \equiv B(\eta_c \to V\,V)/P_V^3$. See, for example, P.A. Carruthers, "Spin and Isospin in Particle Physics," ed. Gordon and Breach, New York (1971).

18. S. Brodsky, private communication.

19. J.D. Jackson, in Proceedings of the 1976 *SLAC Summer Institute on Particle Physics*, ed. by Martha C. Zipf, SLAC-198 (1976) p.147.

Table 1. Branching Ratios of Hadronics Decay Modes of the η_c.

The upper limits are given with a 90% confidence level. The statistical and systematic errors have been combined quadratically. Branching ratios for three- and four-body final states include contributions from two- and three-body intermediate states.

Decay Mode $\eta_c \to X$	Number of Events	Efficiency (%)	Branching Ratio $B(J/\psi \to \gamma\eta_c,\ \eta_c \to X)$	η_c Mass (MeV/c^2)
$\eta\pi^+\pi^-$	75 ± 11	15 ± 3	$(4.6 \pm 1.1) \times 10^{-4}$	2977 ± 4
$\delta^\pm\pi^\mp$	< 14.3		$< 8.8 \times 10^{-5}/B(\delta \to \eta\pi)$	
$f\,\eta$	< 22.9		$< 1.4 \times 10^{-4}$	
$\eta'\pi^+\pi^-$	13.7 ± 3.8	4.8 ± 0.6	$(3.5 \pm 1.1) \times 10^{-4}$	2984 ± 4
$\eta\,K^+K^-$	< 16	7.7 ± 1.4	$< 2.0 \times 10^{-4}$	
$\pi^\pm K^\mp K_S$	63 ± 14	18 ± 2	$(1.9 \pm 0.5) \times 10^{-4}$	2976 ± 5
$\pi^0 K^+K^-$	32 ± 12	9.5 ± 1.6	$(1.3 \pm 0.5) \times 10^{-4}$	2970 ± 7
$\pi^+\pi^-\pi^+\pi^-$	25 ± 9	5.7 ± 0.8	$(1.6 \pm 0.6) \times 10^{-4}$	2982 ± 3
$\rho^0\rho^0$	< 9.3		$< 0.6 \times 10^{-4}$	
$A_2^\pm\pi^\mp$	< 9.3		$< 1.7 \times 10^{-4}$	
$\pi^+\pi^-\,K^+K^-$	110 ± 17	15 ± 2	$(2.7 \pm 0.4) \times 10^{-4}$	2983 ± 5
$\bar{K}^{*0}\,K^-\pi^+ + c.c.$	63 ± 10	14 ± 2	$(2.6 \pm 0.6) \times 10^{-4}$	2982 ± 5
$K^{*0}\,\bar{K}^{*0}$	9 ± 4	13 ± 2	$(0.6 \pm 0.3) \times 10^{-4}$	2969 ± 6
$\omega\omega$	< 5.9	5.6 ± 0.8	$< 3.9 \times 10^{-5}$	
$\phi\phi^\dagger$	16 ± 4	5.8 ± 0.6	$(1.02 \pm 0.29) \times 10^{-4}$	2976 ± 8
$p\bar{p}$	23 ± 11	62 ± 6	$(1.4 \pm 0.7) \times 10^{-5}$	2982 ± 4

† From Ref.7.

Table 2. η_c Branching Ratios.

The branching ratio $B(J/\psi \to \gamma\eta_c)$,[6] used in the determination of $B(\eta_c \to X)$, contributes to a 28% systematic error common to all channels. Upper limits are given at the 90% confidence level. The $\eta_c \to \pi KK$ branching ratio is the average of $B(\eta_c \to \pi^{\pm}K^{\mp}K_S)$ and $B(\eta_c \to \pi^0 K^+K^-)$ (the relevant isospin factors have been taken into account.) Branching ratio for three- and four-body final states include contributions from two- and three-body intermediate states.

Decay Mode $\eta_c \to X$	Branching Ratio $B(\eta_c \to X)$ in percent
$\phi\phi$†	0.8 ± 0.3
K*K*	0.9 ± 0.5
$\rho\rho$	< 1.4
$\omega\omega$	< 0.31
$\delta\pi$	$< 1.0/B(\delta \to \eta\pi)$
$A_2\ \pi$	< 2.0
$f\,\eta$	< 1.1
$\eta\,\pi\pi$	5.4 ± 2.0
$\eta'\pi\pi$	4.1 ± 1.7
πKK	6.1 ± 2.2
$\eta\,KK$	< 3.1
$K^{*0}K^-\pi^+ + c.c.$	2.0 ± 0.5
$\pi^+\pi^-\pi^+\pi^-$	1.3 ± 0.6
$\pi^+\pi^-K^+K^-$	2.1 ± 0.3
$p\bar{p}$	0.11 ± 0.006

† From Ref.7.

FIGURE CAPTIONS

1. Various mechanisms for $\eta_c \to VV$ decay. In (b), the produced mesons are color octet states, but final state interactions (*i.e.* exchange of soft gluons) are assumed to turn them into color singlets.

2. The Mark III detector (a) View transverse to the beam axis. (b) Parallel.

3. The $\eta\pi^+\pi^-$ effective mass distribution for $J/\psi \to \gamma\eta\pi^+\pi^-$ decays. The curve is the result of a fit to a Breit-Wigner convoluted with a Gaussian plus a second order polynomial. The fit does not include events with $\eta\pi^+\pi^-$ effective mass larger than 3.06 GeV/c^2.

4. The $\pi^0 K^+ K^-$ effective mass distribution for $J/\psi \to \gamma K^+ K^- \pi^0$ decays. The curve is the result of a fit to a Breit-Wigner convoluted with a Gaussian plus a second order polynomial.

5. The $\pi^+\pi^-$ effective mass distribution for the pair of tracks selected as K_S, after all cuts, in the decay $J/\psi \to \gamma\ \pi^\pm K^\mp K_S$. The curve is a Gaussian fit to the distribution.

6. The $\pi^\pm K^\mp K_S$ effective mass distribution for $J/\psi \to \gamma K_S K^\pm \pi^\mp$ decays. The curve is the result of a fit to a Breit-Wigner convoluted with a Gaussian plus a second order polynomial.

7. The $\gamma\pi^+\pi^-$ effective mass distribution for events of the type $J/\psi \to \gamma\gamma\pi^+\pi^-\pi^+\pi^-$. The $\pi^+\pi^-$ pair used is the one whose mass is the closest to that of the ρ^0 (2 entries/event).

8. The $\eta'\pi^+\pi^-$ effective mass distributions for $J/\psi \to \gamma\eta'\ \pi^+\pi^-$ decays.

9. The $\pi^+\pi^-\pi^+\pi^-$ effective mass distribution for $J/\psi \to \gamma\pi^+\pi^-\pi^+\pi^-$ decays. Background events from $J/\psi \to \pi^0\pi^+\pi^-\pi^+\pi^-$ decays have been subtracted.[14] The curve is the result of a fit to a Gaussian plus a constant for the background.

10. $J/\psi \to \pi^+\pi^-K^+K^-$ decays: (a) The $\pi^+\pi^-K^+K^-$ effective mass distribution. (b) The $K^{*0}K^-\pi^+$ effective mass distribution (including the conjugate mode $\bar{K}^{*0}K^+\pi^-$.) A $K\pi$ pair is taken to be a K^* if its effective mass is equal to 0.892 GeV/c^2 within 80 MeV/c^2. The nonresonant background from $\pi^+\pi^-K^+K^-$ decays has not been removed. (c) The $K^{*0}\bar{K}^{*0}$ effective mass distribution. Nonresonant backgrounds have not been subtracted. The curves are the results of a fit to a Breit-Wigner, convoluted with a Gaussian, plus a polynomial for the background (see text).

11. Scatterplot of $m_{K^-\pi^+}$ versus $m_{K^+\pi^-}$ for $J/\psi \to \gamma\pi^+\pi^-K^+K^-$ decays.

12. The $\omega\omega$ effective mass distribution for $J/\psi \to \gamma\omega\omega$ decays. The curve corresponds to the 90% $C.L.$ upper limit given in Table 1.

13. The $p\bar{p}$ effective mass distribution for $J/\psi \to \gamma p\bar{p}$ decays. The continuous line is the result of a fit to a Breit-Wigner, convoluted with a Gaussian, plus a polynomial for the background. The dashed line is a low estimate of the $J/\psi \to p\bar{p}$ background, and the broken-dashed line is a low estimate of the nonresonant $J/\psi \to \gamma p\bar{p}$ background.

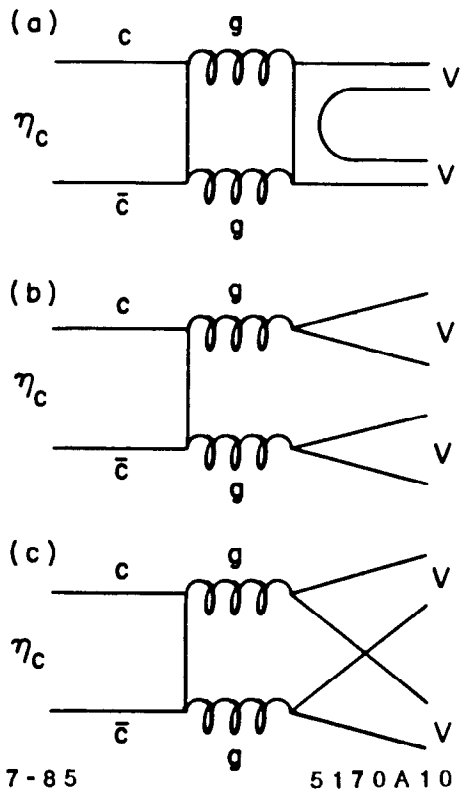
(a)
c
g
V
η_c
V
$\bar{c}$
g
(b)
c
g
V
η_c
V
$\bar{c}$
g
(c)
c
g
V
η_c
V
$\bar{c}$
g
7-85
5170A10

Fig. 1

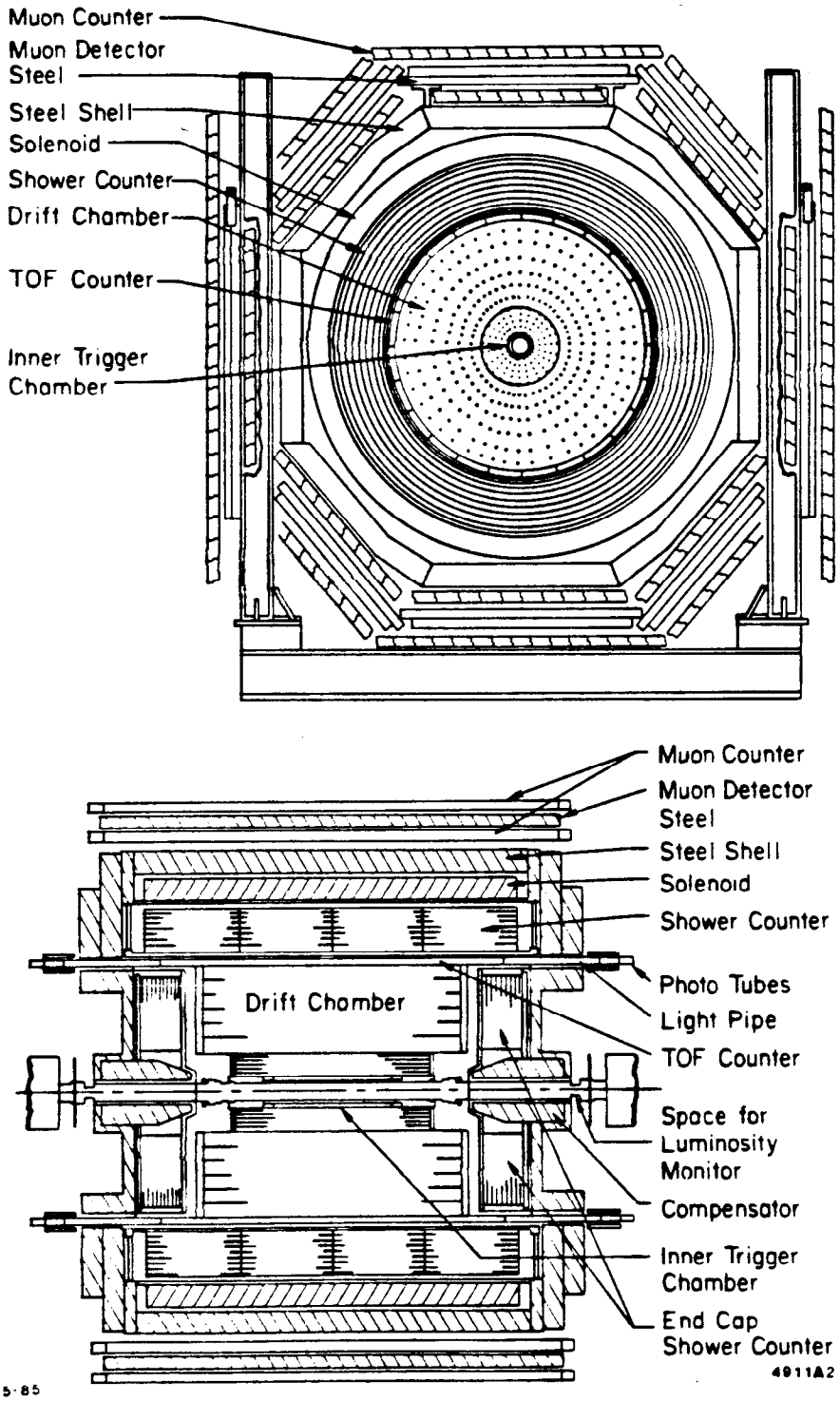
Muon Counter
Muon Detector Steel
Steel Shell
Solenoid
Shower Counter
Drift Chamber
TOF Counter
Inner Trigger Chamber
Muon Counter
Muon Detector Steel
Steel Shell
Solenoid
Shower Counter
Photo Tubes
Light Pipe
TOF Counter
Drift Chamber
Space for Luminosity Monitor
Compensator
Inner Trigger Chamber
End Cap Shower Counter
5-85
4911A2

Fig. 2

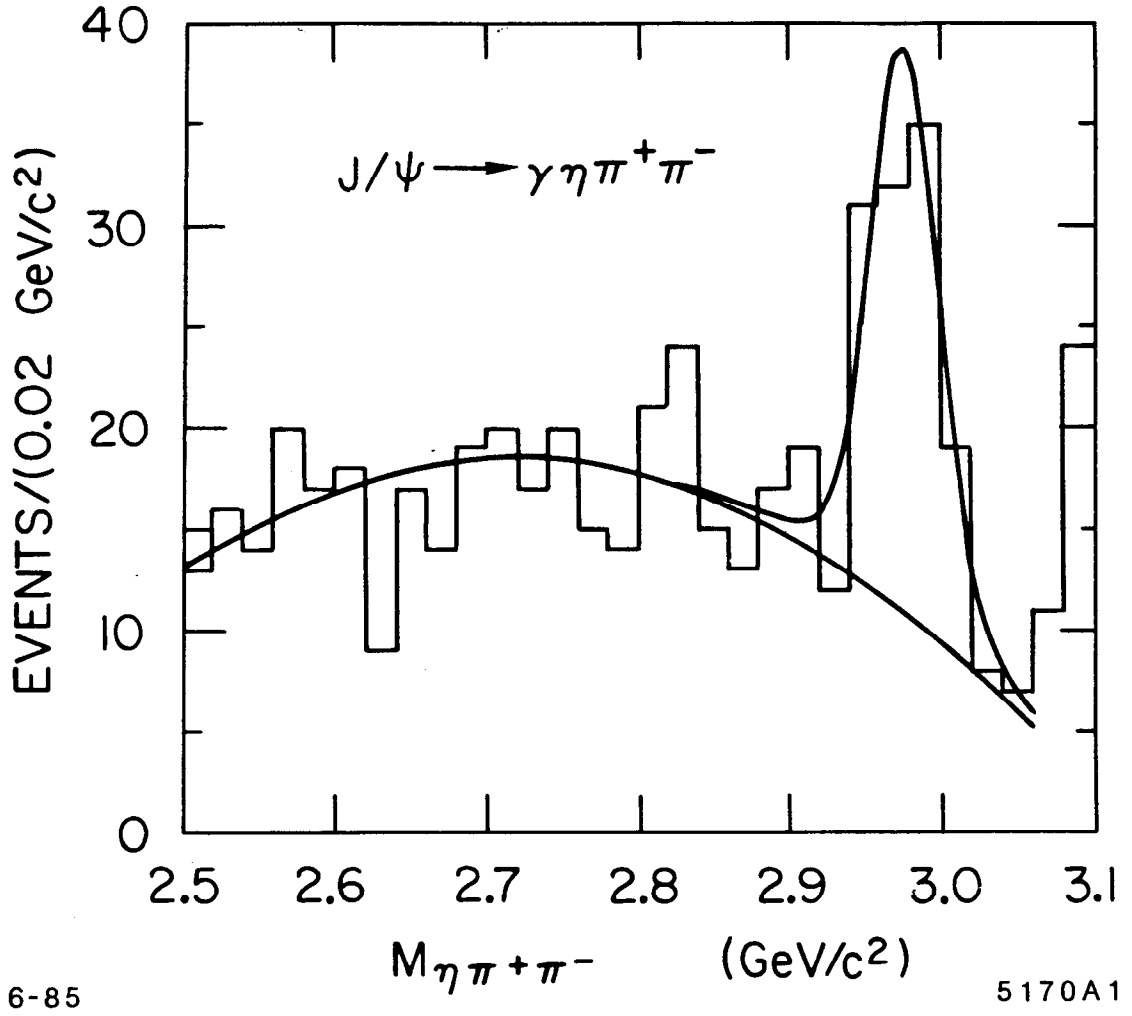
40
30
20
10
0
EVENTS/(0.02 GeV/c²)
J/ψ → γηπ⁺π⁻
2.5
2.6
2.7
2.8
2.9
3.0
3.1
Mηπ⁺π⁻ (GeV/c²)
6-85
5170A1

Fig. 3

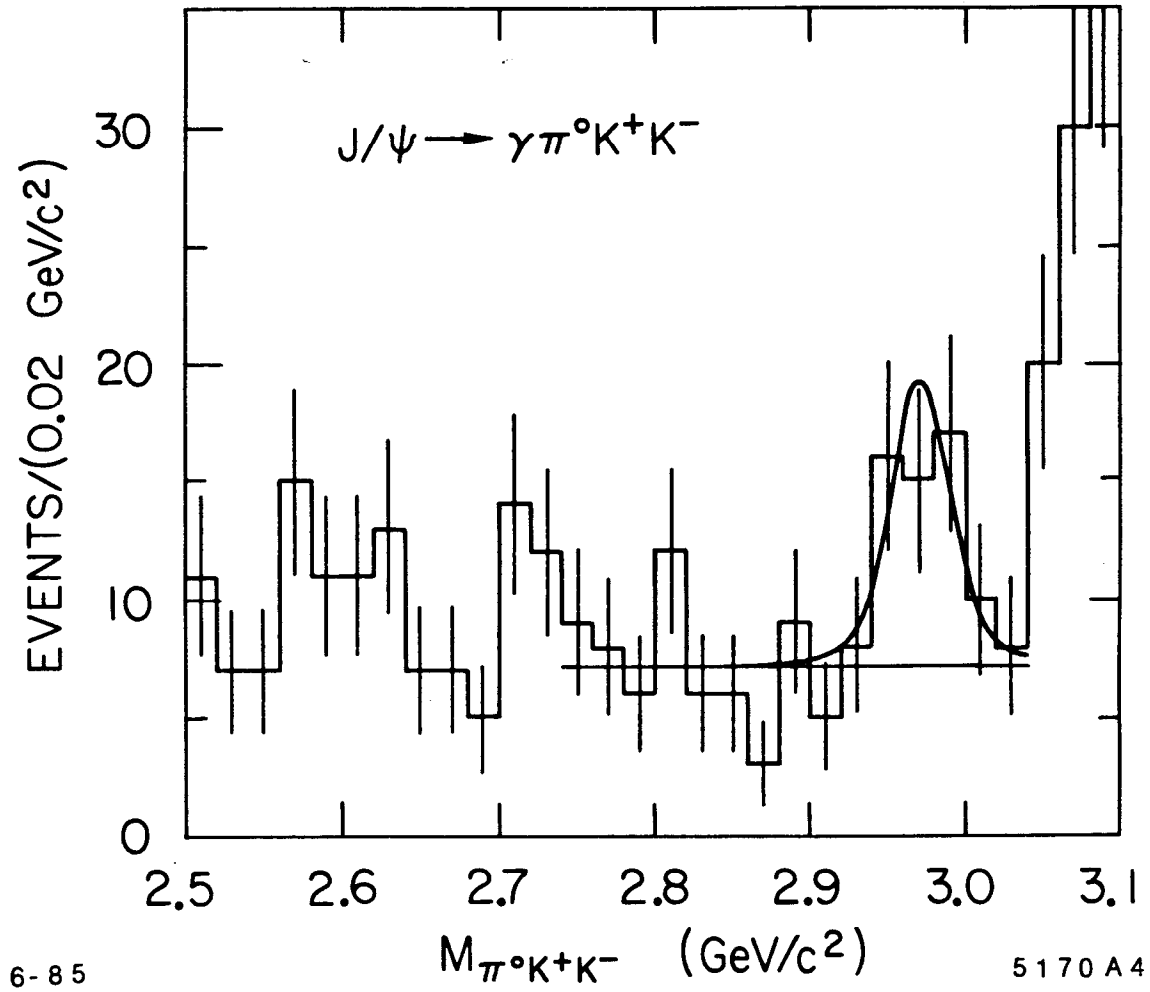
J/ψ → γπ°K+K−
EVENTS/(0.02 GeV/c2)
30
20
10
0
2.5
2.6
2.7
2.8
2.9
3.0
3.1
Mπ°K+K− (GeV/c2)
6-85
5170A4

Fig. 4

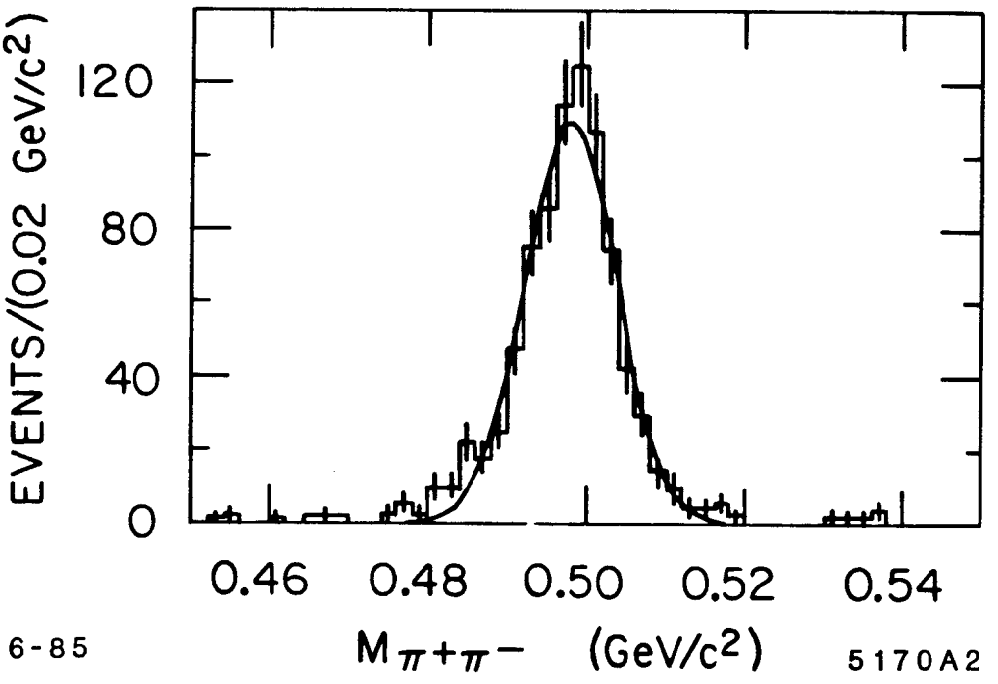
EVENTS/(0.02 GeV/c²)
120
80
40
0
0.46
0.48
0.50
0.52
0.54
6-85
Mπ+π− (GeV/c²)
5170A2

Fig. 5

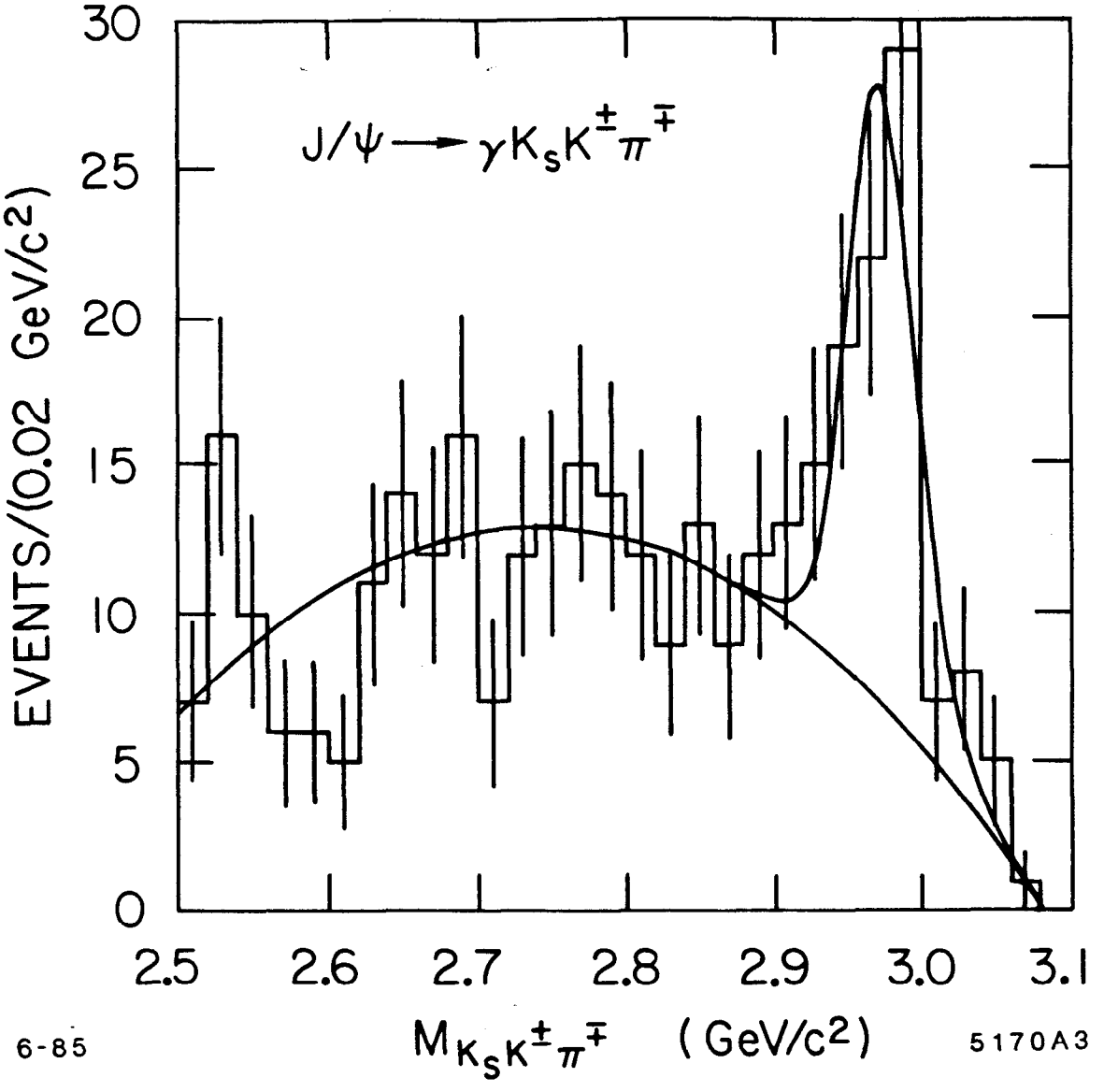
30
25
20
15
10
5
0
EVENTS/(0.02 GeV/c²)
J/ψ → γK_sK^±π^∓
2.5
2.6
2.7
2.8
2.9
3.0
3.1
M_K_sK^±π^∓ (GeV/c²)
6-85
5170A3

Fig. 6

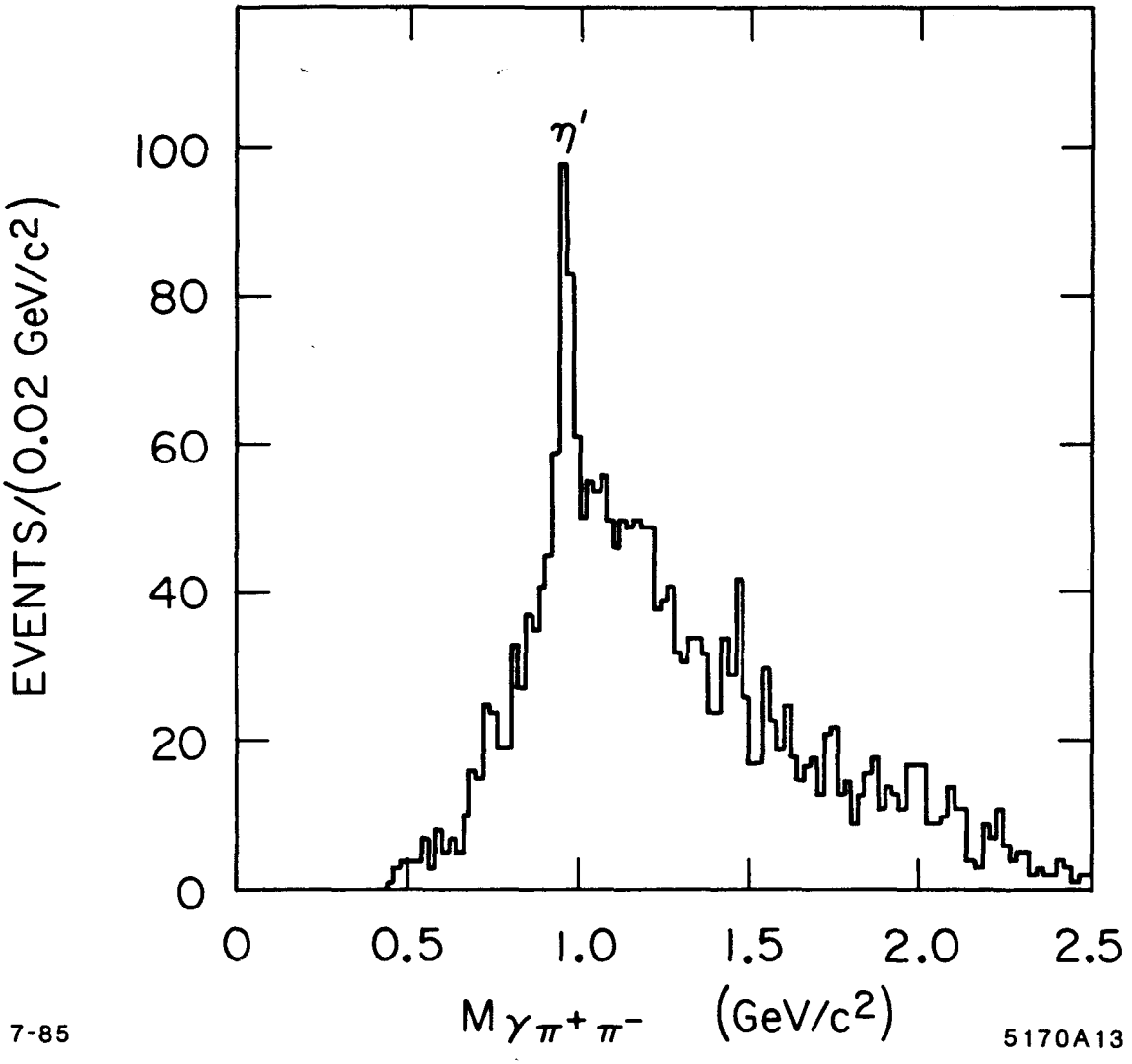
EVENTS/(0.02 GeV/c²)
100
80
60
40
20
0
η'
0
0.5
1.0
1.5
2.0
2.5
M γπ+π−
(GeV/c²)
7-85
5170A13

Fig. 7

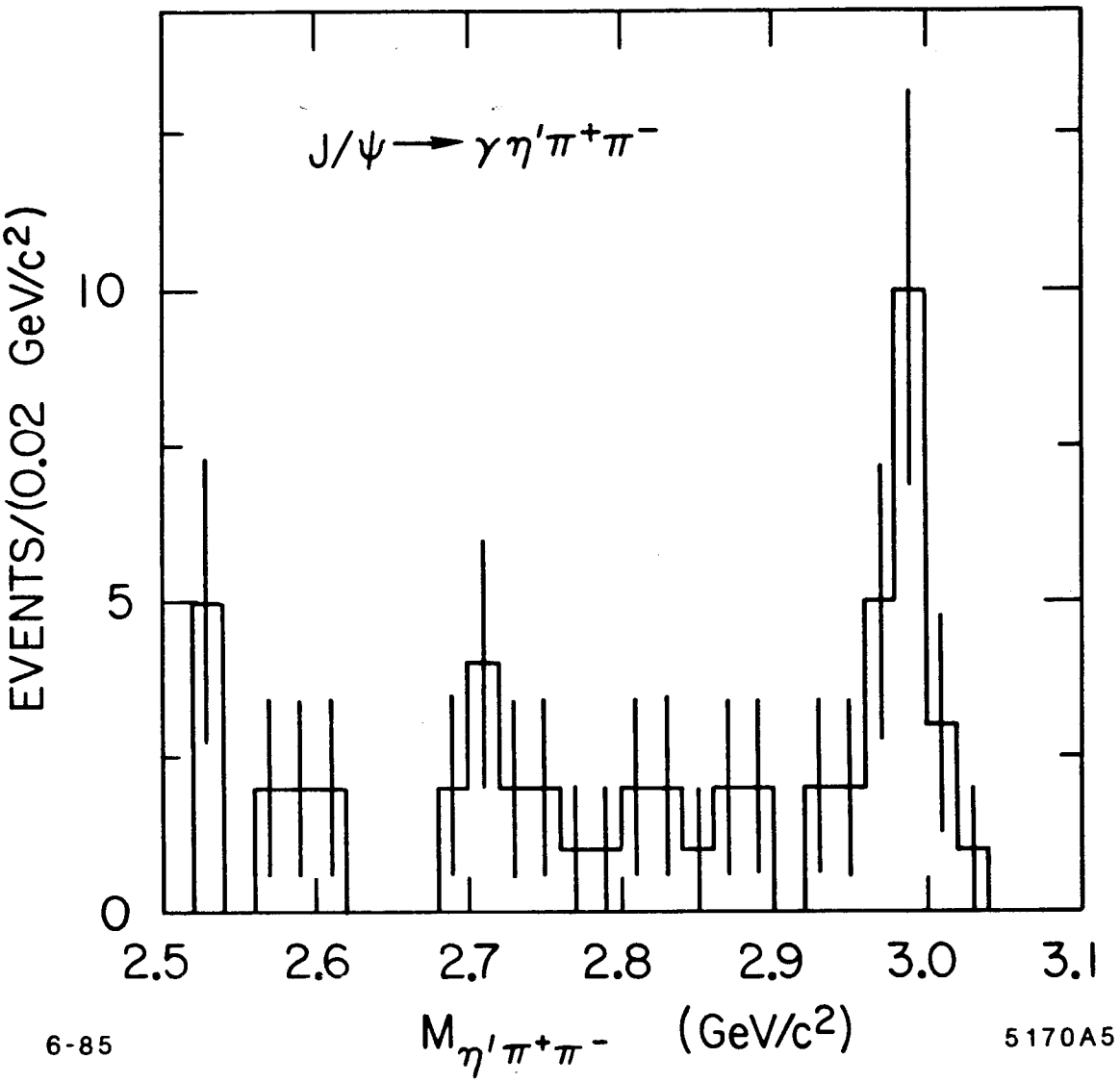
J/ψ → γη'π+π−
EVENTS/(0.02 GeV/c2)
10
5
0
2.5
2.6
2.7
2.8
2.9
3.0
3.1
Mη'π+π− (GeV/c2)
6-85
5170A5

Fig. 8

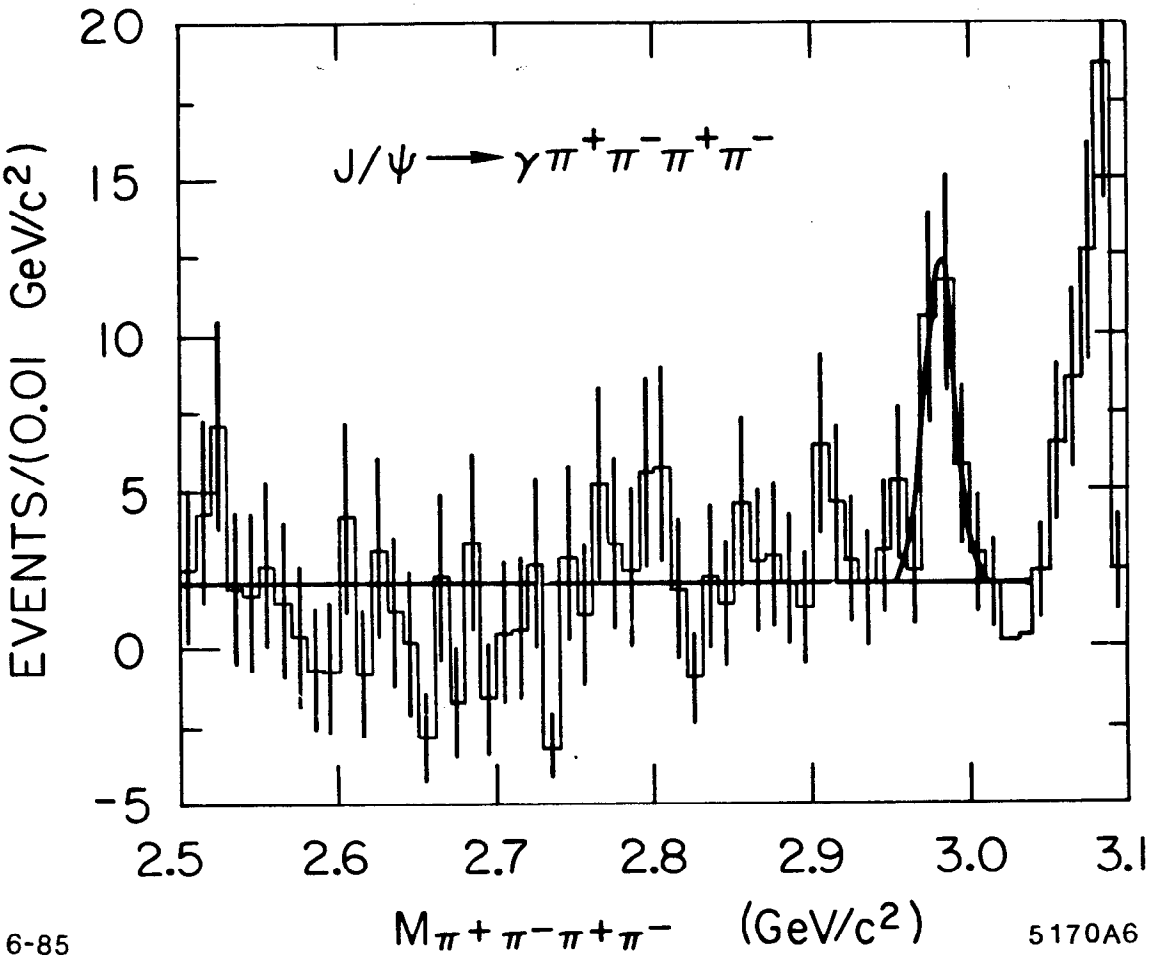
20
15
10
5
0
-5
EVENTS/(0.01 GeV/c²)
J/ψ → γπ⁺π⁻π⁺π⁻
2.5
2.6
2.7
2.8
2.9
3.0
3.1
Mπ+π−π+π− (GeV/c²)
6-85
5170A6

Fig. 9

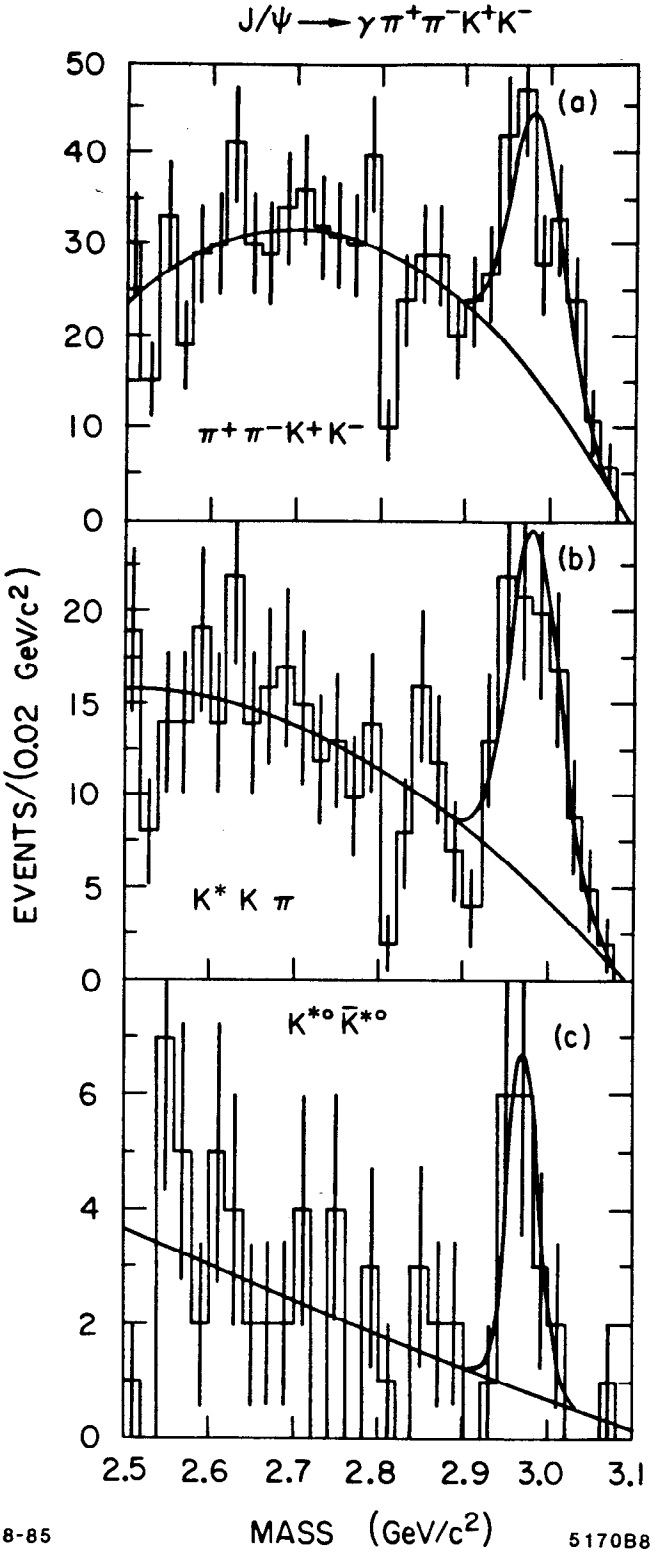
J/ψ → γπ+π−K+K−
(a)
π+π−K+K−
(b)
K* K π
(c)
K*° K̄*°
EVENTS/(0.02 GeV/c²)
MASS (GeV/c²)
8-85
5170B8

Fig. 10

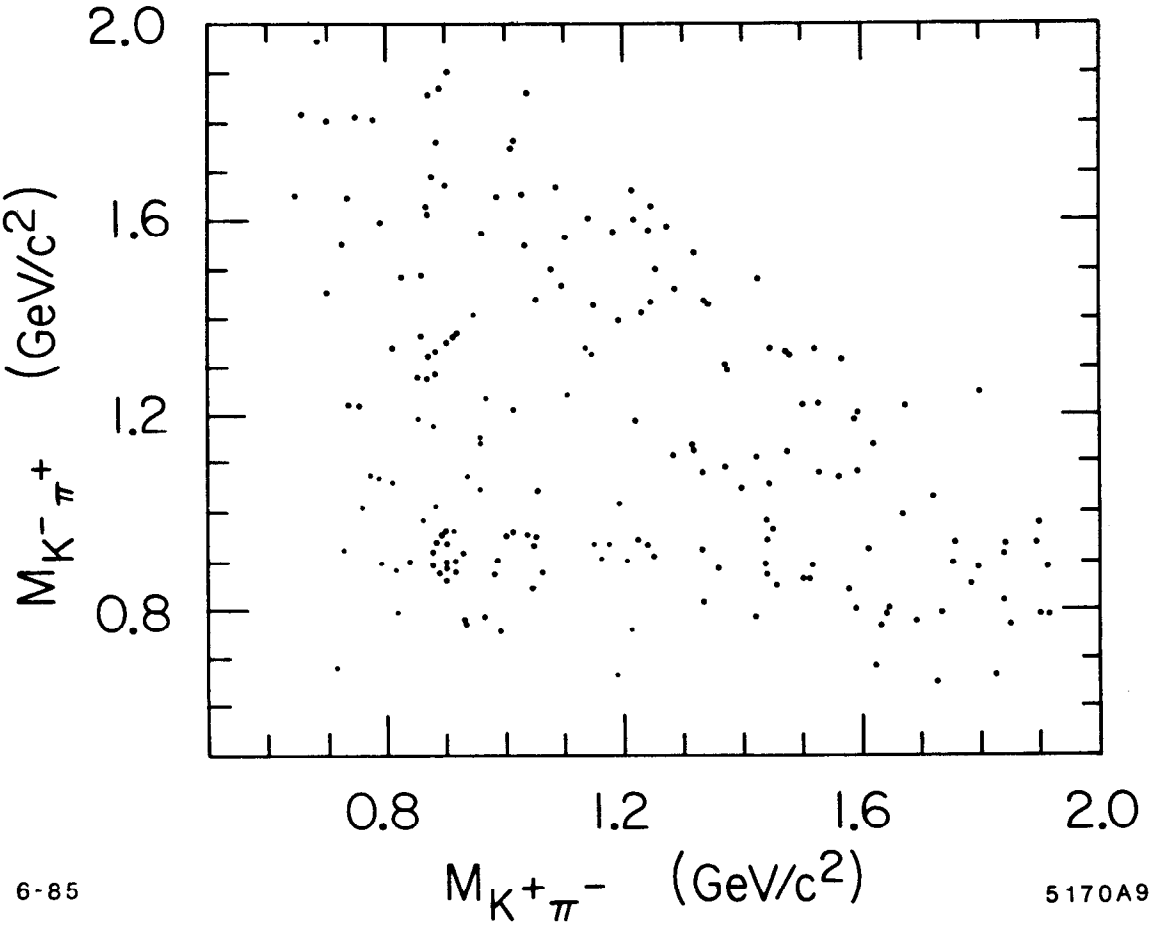

Fig. 11

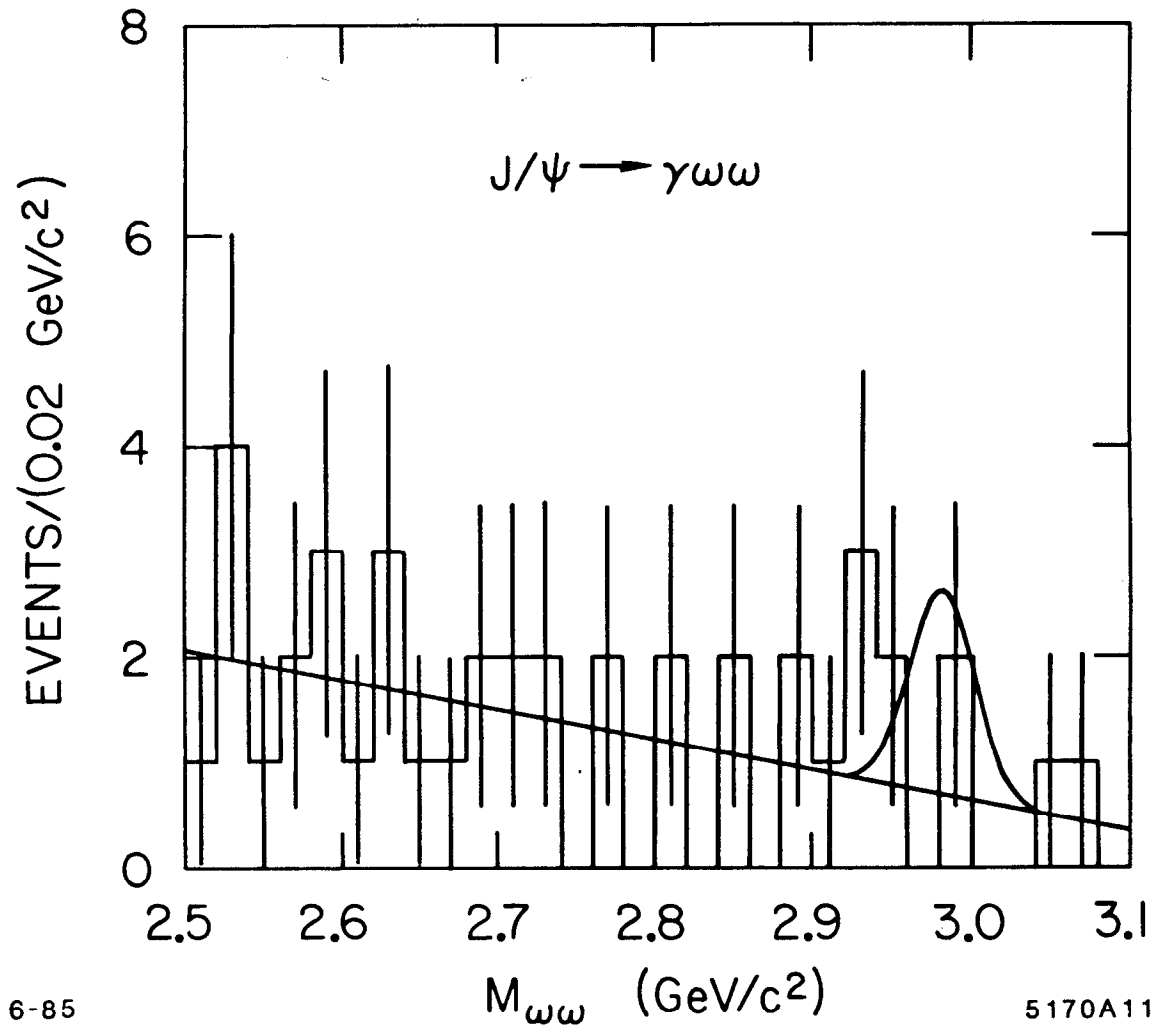
8
6
4
2
0
EVENTS/(0.02 GeV/c²)
J/ψ → γωω
2.5
2.6
2.7
2.8
2.9
3.0
3.1
Mωω (GeV/c²)
6-85
5170A11

Fig. 12

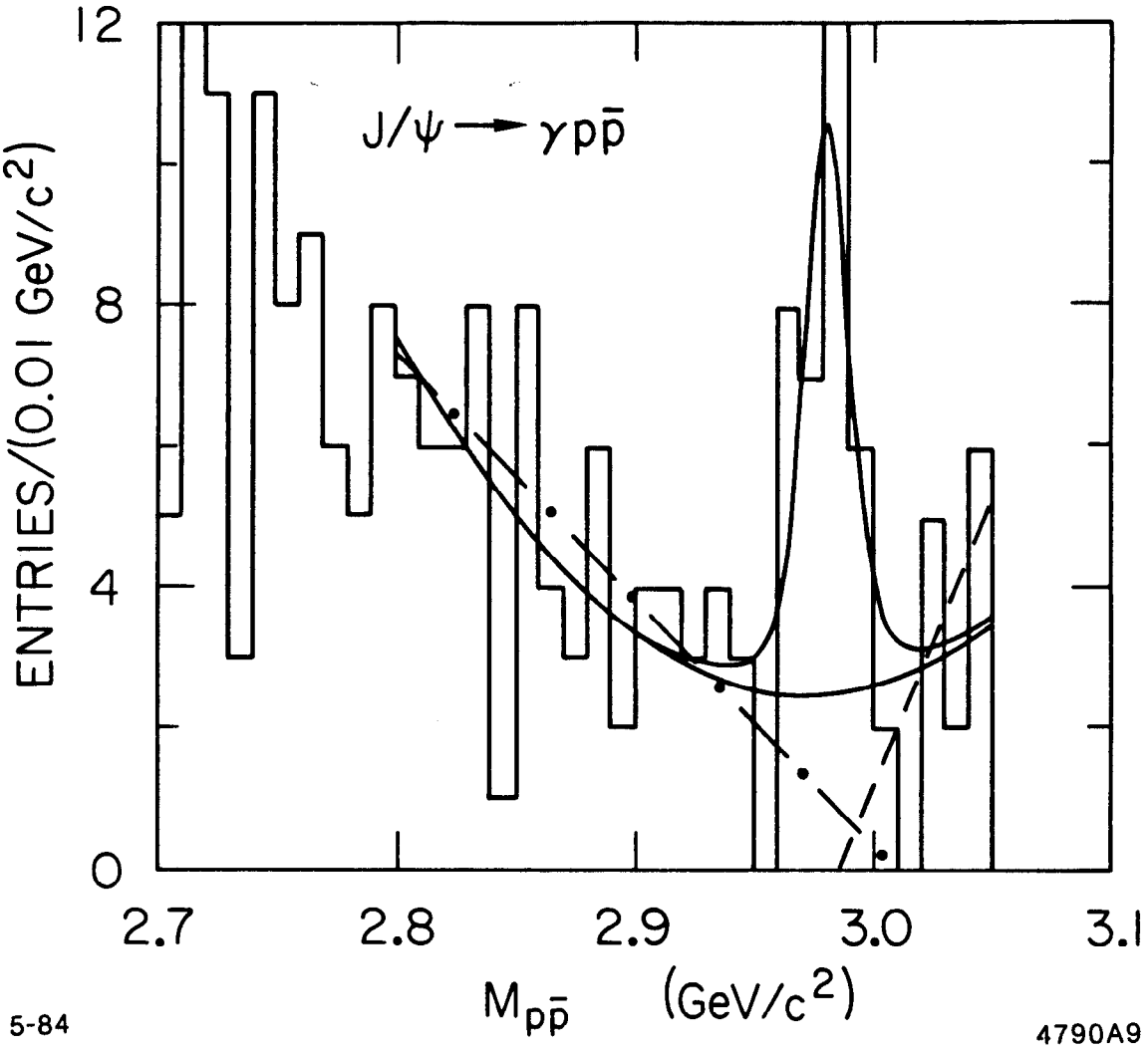
12
8
4
0
ENTRIES/(0.01 GeV/c²)
J/ψ → γpp̄
2.7
2.8
2.9
3.0
3.1
M_pp̄ (GeV/c²)
5-84
4790A9

Fig. 13